First published online as a Review in Advance on February 6, 2007

Small-Angle X-ray Scattering from RNA, Proteins, and Protein Complexes

Jan Lipfert[1] and Sebastian Doniach[1,2]

[1]Departments of Physics and [2]Applied Physics, Biophysics Program, and Stanford Synchrotron Radiation Laboratory, Stanford University, Stanford, California 94305; email: lipfert@stanford.edu; doniach@drizzle.stanford.edu

Annu. Rev. Biophys. Biomol. Struct. 2007. 36:307–27

The *Annual Review of Biophysics and Biomolecular Structure* is online at biophys.annualreviews.org

This article's doi: 10.1146/annurev.biophys.36.040306.132655

1056-8700/07/0609-0307$20.00

Key Words

SAXS, membrane proteins, unfolded proteins, molecular reconstruction

Abstract

Small-angle X-ray scattering (SAXS) is increasingly used to characterize the structure and interactions of biological macromolecules and their complexes in solution. Although still a low-resolution technique, the advent of high-flux synchrotron sources and the development of algorithms for the reconstruction of 3-D electron density maps from 1-D scattering profiles have made possible the generation of useful low-resolution molecular models from SAXS data. Furthermore, SAXS is well suited for the study of unfolded or partially folded conformational ensembles as a function of time or solution conditions. Here, we review recently developed algorithms for 3-D structure modeling and applications to protein complexes. Furthermore, we discuss the emerging use of SAXS as a tool to study membrane protein-detergent complexes. SAXS is proving useful to study the folding of functional RNA molecules, and finally we discuss uses of SAXS to study ensembles of denatured proteins.

Contents

INTRODUCTION

Small-angle X-ray scattering (SAXS) is a technique that allows the study of the structure and interactions of biological macromolecules in solution. SAXS can be used to probe proteins, nucleic acids, and their complexes under a variety of conditions, from (near-) physiological to highly denaturing, without the need to crystallize the sample and without the molecular weight limitations inherent in other methods such as NMR spectroscopy. The increasing availability of high-flux, third-generation synchrotron sources, improvements in detector hardware, and algorithmic developments for data analysis have made SAXS a technique of choice for a range of biological applications. The growing importance of SAXS as a tool in structural biology is reflected in the number of SAXS-related publications per year, which has tripled in the past decade (36).

The basic principle of SAXS is to scatter X-ray photons elastically off molecules in solution and to record the scattering intensity as a function of the scattering angle. **Figure 1** shows a schematic of a typical SAXS measurement. The recorded scattering profile provides information about the global structure and conformation of the studied molecules. Historically, SAXS has been used to obtain a few key parameters such as the molecular weight *MW*, radius of gyration R_g, and maximum intramolecular distance D_{max} (34, 37). Several excellent reviews on the physical principles and theory of SAXS describe in detail how the scattering data can be analyzed and how different parameters can be fit and interpreted (26, 34, 46, 93). In this review, we therefore focus on more recent developments and novel applications of SAXS and only briefly discuss the basic physical principles to highlight the challenges unique to different experimental targets.

The past decade has seen the development of algorithms that allow ab initio reconstructions of low-resolution 3-D electron density

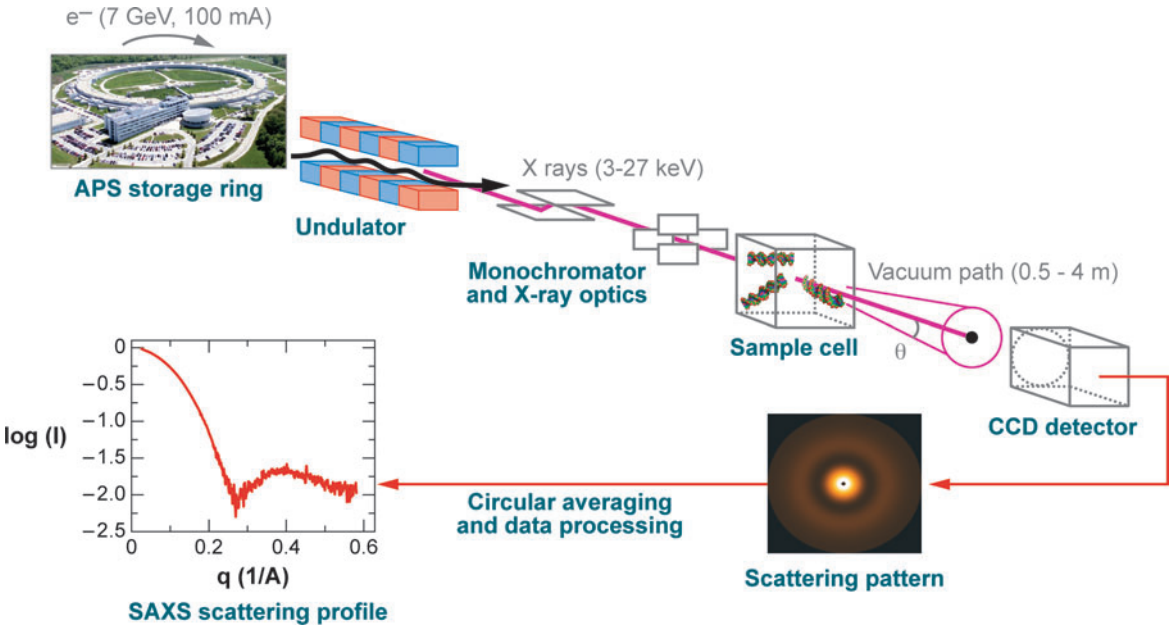

Figure 1

Schematic small-angle X-ray scattering setup for beam line 12-ID at the Advanced Photon Source (APS). The SAXS intensity is typically recorded as a function of momentum transfer q, $q = 4\pi \sin(\theta)/\lambda$, where 2θ is the total scattering angle and λ is the X-ray wavelength. Details of the measurement setup have been described in References 7, 61, and 83.

maps from 1-D scattering profiles (18, 92, 94, 104), allowing one to obtain structural information beyond simple parameters such as the R_g. Recently, Svergun and coworkers have created tools to model molecular complexes from SAXS data if the structures of the individual components are (partially) known from higher resolution experiments (49, 70, 72). We review these algorithms and recent applications to molecular complexes (see 3-D Reconstructions, below).

Membrane proteins have received much attention for their importance in cell metabolism and as drug targets; however, they lead to significant challenges for most structural techniques (79, 105). One of the main obstacles is the need to solubilize membrane proteins, which is most often accomplished by micelle-forming detergents. Recent advances in the study of the resulting protein-detergent complexes (PDCs) by SAXS are reviewed (see Membrane Proteins and Protein-Detergent Complexes, below).

The discovery in the early 1980s that RNA can act as an enzyme or ribozyme (32) and the more recent realization that RNA not only carries genetic information as mRNA, but is also highly involved in the regulation of that information (64, 87) have led to a surge in interest in RNA structural biology. We review the important contributions that SAXS has made to our understanding of RNA folding as well as the current trends in the field (see Nucleic Acids, below).

SAXS has been an important technique for the investigation of the conformational ensembles populated by unfolded proteins under highly denaturing conditions (26, 67). The global structure of denatured proteins as measured by R_g appears consistent with a simple Flory picture of a self-avoiding random walk. However, recent experiments have suggested

Small-angle X-ray scattering (SAXS): experimental technique that records the scattered X-ray photons from noncrystalline samples (in particular biological macromolecules in solution)

Radius of gyration: measure for the overall size of a macromolecule, computed as the weighted average of square center-of-mass distances in the molecule

Micelle: an aggregate of detergent molecules; in aqueous solution hydrophilic head groups face outward and hydrophobic tail groups are sequestered in the interior

Protein-detergent complex (PDC): molecular complex formed by one or more membrane proteins and detergent molecules

residual structure even under highly denaturing conditions (66, 84) and have seen significant deviations from predictions of molecular dynamics simulations (111). These results bring up significant outstanding questions regarding our current understanding of the unfolded state (see Unfolded Proteins and Peptides, below).

3-D RECONSTRUCTIONS

The parameters most frequently extracted from a SAXS profile for a biomolecule in solution (which is sufficiently dilute to avoid the effects of interparticle interference) are R_g and forward scattering intensity $I(0)$. They are obtained from the Guinier formula $I(q) \approx I(0)\exp(-q^2 R_g^2/3)$, for small momentum transfer q ($q = 4\pi \sin(\theta)/\lambda$, where 2θ is the total scattering angle and λ the X-ray wavelength), by plotting $\ln(I(q))$ versus q^2 and fitting the slope and intercept (34, 37). R_g is a model free characterization of the molecular size and $I(0)$ can be related to the molecular weight with the relation

$$I(0) = \kappa c(\Delta\rho)^2(MW)^2, \qquad 1.$$

where κ is a proportionality constant that can be determined from a measurement of a molecular weight standard (e.g., a protein of known molecular weight and concentration), c is the concentration of the macromolecule, $\Delta\rho$ is the average electron density contrast of the molecule, and MW is the molecular weight.

More generally the scattering profile maybe written in terms of the distribution function $p(r)$ of intramolecular atomic distances (D_{max} being the maximum intramolecular distance):

$$I(q) = \int_0^{D_{max}} dr p(r) \frac{\sin(qr)}{qr}. \qquad 2.$$

$p(r)$ can be obtained from an indirect Fourier transform of the scattering profile, e.g., using the software GNOM by Svergun (91), which employs the regularization procedure of Tikhonov & Arsenin (101). However, in recent years the use of $p(r)$ to help visualize the molecular shape has been superseded by algorithms that provide a low-resolution 3-D electron density map of the molecule from the 1-D SAXS profile.

Ab Initio Determination of Molecular Shape

Owing to the physical constraint that a biomolecule in general has a rather uniform electron density, Stuhrmann proposed representing the scattering profile in terms of a spherical harmonic expansion of the molecular surface (88, 89, 95). Determination of the coefficients of the spherical harmonics by a nonlinear, least-squares fitting procedure to the data led to the ab initio determination of the molecular shape. However, in practice this limits the shapes that can be considered to molecules close in shape to a deformed sphere. Molecules with multiple domains and/or cavities cannot be represented in this simple spherical harmonic expansion.

In 1998 Chacon et al. (18) showed that models in which the molecular electron density is approximated in terms of an assembly of beads or dummy atoms (represented as point scatterers) can be used to fit to the scattering data. It is advantageous to incorporate physical constraints, such as imposing a uniform density on the interior of the molecule, into the fitting procedure in addition to the experimental scattering data. The fit leads to a multidimensional minimization problem that can be numerically solved by using various Monte Carlo–like procedures. Chacon's method, termed Dalai GA, uses a genetic algorithm (18). Svergun and coworkers have developed DAMMIN (92), a simulated annealing procedure that imposes a compactness criterion, and GASBOR (71, 94), a program that specializes the DAMMIN routine for the reconstructions of proteins (available online at **http://www.embl-hamburg.de/ExternalInfo/Research/Sax/software.html**). Walther et al. (104) use a "give'n'take" algorithm in their software

saxs3d (available online at **http://www.cmpharm.ucsf.edu/~walther/saxs/**). Fujisawa and coworkers (96) have compared these methods.

However, the reconstruction of a 3-D density from a 1-D scattering profile is not unique. Alternative solutions involving structural partners for a given 3-D reconstruction cannot in general be avoided, owing to the lack of phase and angular orientation information inherent in SAXS measurements. Structural partners are bead-model solutions with different geometries that give nearly identical $I(q)$ solutions. Such partners occur most readily for shapes of high symmetry such as cylinders. In practice, it is advantageous to compare and average the results of different reconstruction runs to assess the uniqueness of the solutions and to improve the robustness of the fit. Svergun and coworkers (51, 102) have created a software package that compares models on the basis of a normalized spatial discrepancy criterion and implements an averaging procedure. Another useful software is Situs by Wriggers and coworkers (107, 108), which is a suite of programs that converts the bead models into standard density map formats and to dock known atomic resolution structures into the reconstructed densities (available online at **http://situs.biomachina.org/**).

What Are the Limitations of Spatial Resolution for Bead Models?

In order to assess the number of beads that should be used and the spatial resolution that can be achieved in a 3-D reconstruction, the concept of model noise is useful. Kretchetov (53) found that small changes in the bead positions of a given bead model can lead to large changes in the histogram of bead-bead distances [a low-resolution representation of $p(r)$] at small r. He developed a procedure in which an ensemble of bead models with a fixed number N of beads for a molecule of given shape Γ is generated. For each member of the ensemble, N beads are placed randomly within the shell Γ with an average spacing $a_{\text{bead-bead}}$ corresponding to the bead density for a given N. An ensemble of $I(q)$ functions may then be generated from the ensemble of bead models, and a mean $\langle I(q)\rangle$ and variance can be evaluated. By comparing the variance of the model as a function of q with the variance of the experimental $I_{\text{ex}}(q)$, an optimal value of N can be determined that is justified by the data. Use of a larger number of beads would not be justified because the model noise would then be smaller than the data noise. Similarly use of too few beads would lead to model noise bigger than the data noise. The resulting mean bead spacing, $a_{\text{bead-bead}}$, provides an estimate of the spatial resolution of the model. In practice the effective resolution of bead models derived from experimental SAXS data can vary from ~5 Å in the case of small molecules ($R_g \lesssim 15$ Å), with data having a good signal/noise ratio, to ~15 Å for larger molecules ($R_g \approx 75$ Å).

Examples of Ab Initio Determination of Molecular Structures

The work of Bada et al. (3) on the yeast switch protein serves as an example of how 3-D reconstructions can help build a molecular model. The sequence and function information of the protein already suggested the existence of a DNA binding domain and of a coiled-coil domain extending away from the DNA binding domain. A 3-D reconstruction from SAXS data using the algorithm saxs3d showed that the molecule has an overall broom shape in which the coiled-coil handle extends some 108 Å from the DNA binding domain. On the basis of this shape information, a low-resolution model was assembled by associating the shape of the lambda repressor DNA binding domain, and a coiled-coil handle modeled from the known structure of collagen (see **Figure 2**). Models of this type, while speculative, are useful for forming hypotheses about the function of the given molecule. In this case the sequence of the distal end of the coiled-coil handle domain contains an actin binding sequence, leading

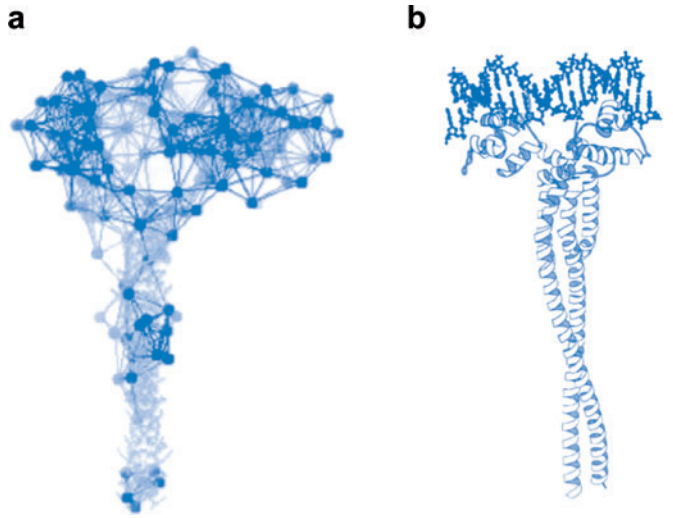

Figure 2

Models of SAP-1 DNA binding protein complexed with DNA oligomer (Reprinted from Reference 3 with permission from Elsevier). Reconstruction from SAXS data using saxs3d (*a*) and model built from homologous fragments (*b*).

to the hypothesis that the cytoskeleton is involved in the switching mechanism of the enzyme.

Other examples of applications of ab initio structure modeling include a combined SAXS and crystallography study of β-mannosidase (2), two (somewhat conflicting) studies of lipoxygenases (22, 38), work on the oligomerization and ligand-binding-associated conformational changes of the two retinoic acid receptors RXR and RAR (30), and a characterization of tropomodulin (31). Recent applications to the reconstruction of RNA structures are discussed below.

Modeling of Molecular Complexes from SAXS Data

An important challenge in structural biology is the determination of the quaternary structure of molecular complexes. Svergun and coworkers have created a suite of programs for the modeling of molecular complexes that incorporates different kinds of a priori information (**http://www.embl-hamburg.de/ExternalInfo/Research/Sax/software.html**). Molecular modeling is generally greatly facilitated if prior knowledge from different techniques can be incorporated. In particular favorable cases, high-resolution structures for the components of a quaternary complex are available. The programs ASSA and MASHA (49, 50) can be used for manual rigid-body manipulation of the components. An automated rigid-body fitting procedure that incorporates different kinds of geometric constraints from prior knowledge is described in Reference 72. It is also possible to combine rigid-body fitting with ab initio reconstructions for cases in which high-resolution structures are partially available but parts of the complex (e.g., flexible linkers) are missing.

An example of this type of modeling is the work of Costenaro et al. (21) on the solution structure of the full length DNA gyrase A subunit. DNA gyrase from *Escherichia coli* consists of two subunits, GyrA (97 kDa) and GyrB (90 kDa), the active enzyme being a heterotetramer A2B2. The subunit GyrA consists of two domains: an amino-terminal domain of 59 kDa (GyrA59) whose structure is known from crystallography (68) and a carboxyl-terminal domain of 38 kDa (GyrA-CTD). GyrA59 contains the active-site tyrosine (Tyr122) residues responsible for the cleavage and religation activity of gyrase. Its structure shows a heart-shaped arrangement with two dimer interfaces (see blue domain in **Figure 3**). The amino-terminal interface forms a positively charged saddle-like surface with the two active-site tyrosines lying near the center. This surface is thought to be the binding region for duplex DNA (the G segment) and to form the DNA gate. The authors use the 3-D reconstruction algorithms GASBOR and CREDO (70) to obtain low-resolution models of the full-length A subunit. In doing so they generate a number of structural partners. To help obtain a consensus solution, they fix the known structure of the GyrA59 domain and use CREDO to refine the bead model for the carboxyl-terminal domain. (In GASBOR and CREDO each bead

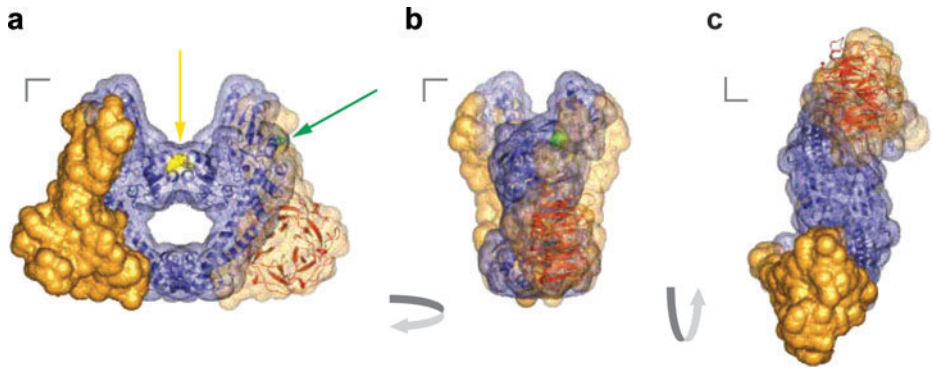

Figure 3

GyrA solution structure (Reprinted from Reference 21 with permission from Elsevier). The model obtained with CREDO is represented as a surface with the fixed GyrA59 structure (*blue*) (68) and the added densities for GyrA-CTD on both sides (*orange*). The active-site tyrosines are colored in yellow and the GyrA59 carboxyl in green, shown in space fill, and indicated by arrows in (*a*). The surface was built from a sphere radius of 5 Å for each residue. The GyrA59 crystallographic structure is shown in blue ribbons. The red ribbons represent the six-bladed β pinwheel domain of one GyrA-CTD (carboxyl-terminal domain), modeled from a homologous crystallographic structure (20) and fitted into the density added by CREDO. The views (*a–c*) are from (*a*) front, (*b*) side, and (*c*) bottom. The x axis is in red, y in green, and z in blue; their length is 10 Å.

corresponds to a residue. However, there is no sequence information, so the bead positions only give a correct average residue density without locating specific residues.) From the resulting model (see **Figure 3**) the authors conclude that the position of the carboxyl-terminal domain strongly suggests a large conformational change of the enzyme for wrapping the DNA on binding for supercoiling. Other recent examples of model building for molecular complexes include a study of the hepatocyte growth factor/scattering factor (33) and a combined SAXS and crystallography study of the Ca^{2+}/calmodulin-dependent protein kinase II (75).

The Problem of Incorporating Sequence Information into 3-D Reconstructions Obtained from SAXS Data

It is tempting to assume that knowledge of the sequence of a protein is sufficient to assign the beads used in the reconstruction to specific residues in the protein. However, this is not the case. SAXS yields a histogram of pair distances, but the identities of the pairs contributing to a given bin of the histogram are not known (unlike in the case for NMR data). Zheng & Doniach (113) evaluated the use of SAXS data to filter candidate models generated from ab initio protein structure prediction algorithms. The SAXS data provide significant spatial constraints that allow the rejection of large numbers of false positives. However, the overall improvement in the success rate for ab initio structure prediction was found to be limited. Recently, Ma and coworkers (109) have reported the use of SAXS data as a weak guiding constraint in protein folding simulations of small helical proteins.

MEMBRANE PROTEINS AND PROTEIN-DETERGENT COMPLEXES

Membrane proteins are located in the cell membranes, where they are involved in a range of important cellular functions. Whereas membrane proteins constitute an

Small-angle neutron scattering (SANS): technique similar to SAXS in which neutrons are used instead of X-ray photons

estimated 30–40% of all genes (103) and approximately 50% of all drug targets (48), less than 1% of the structures currently deposited in the Protein Data Bank (8) are of membrane proteins.

A major hurdle to structural studies is the need to solubilize membrane proteins (105). Micelle-forming detergents are routinely used to encapsulate the hydrophobic transmembrane regions of the protein and to act as a mimetic of the cell membrane. This detergent sheath in the PDC adds considerable complexity to structural studies of membrane proteins, as each step in preparation, purification, and characterization of the protein-detergent conditions needs to be optimized to ensure solubility. In particular, the presence of detergents complicates crystallization attempts, making it difficult to obtain good-quality crystals for X-ray crystallography. Furthermore, the added molecular weight from the detergent layer as well as protein-detergent interactions make NMR studies of membrane proteins challenging (79).

SAXS (28, 43, 112) and small-angle neutron scattering (SANS) (6, 10, 42, 57, 100) have been used extensively to characterize the shape, size, and interactions of empty detergent micelles, lipid vesicles (11, 13), and self-assembled lipid-protein nanodiscs (25). The approach in these studies has been generally to model the scattering intensity using simple geometric shapes, such as two-component spheres (42), ellipsoids (6, 10, 28, 57), or cylinders (112), whose parameters are fit against the experimental data. Some of the studies have included finite-concentration interparticle interference effects, explicitly using simple models for interparticle interactions (39, 41).

A major challenge in the study of PDCs by SAXS is the need to separate the scattering signal from the PDC from that of the empty micelles that are also present in solution (see **Figure 4**). Several strategies have been

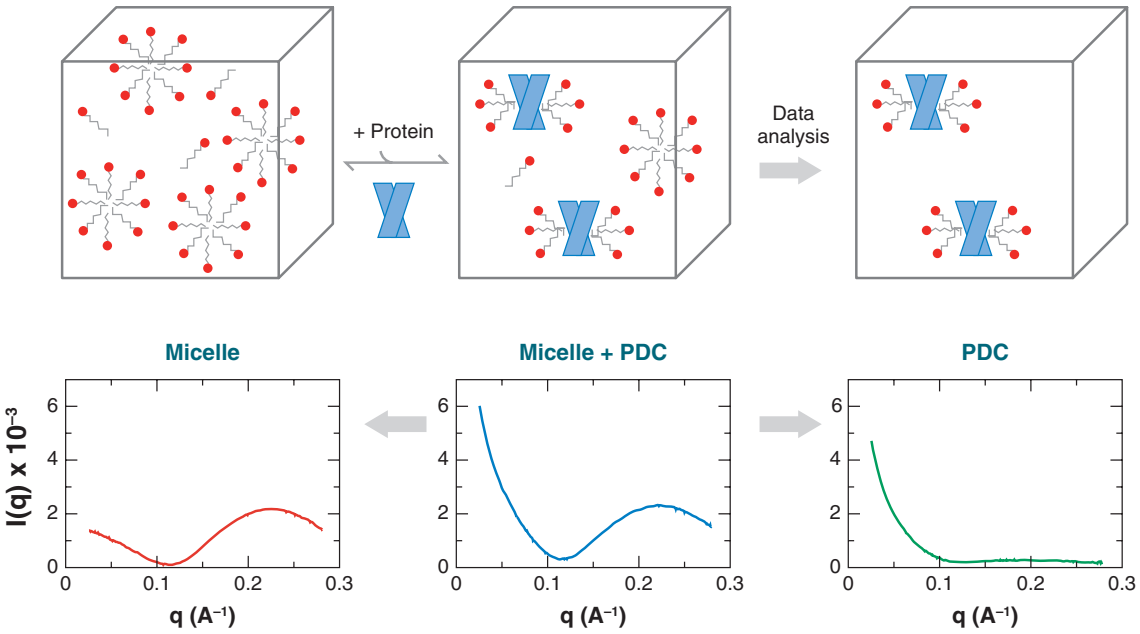

Figure 4

Schematic of a SAXS experiment to determine the scattering profile of a protein detergent complex (PDC). The scattering profiles of the detergent micelles (*left*) and of the protein-detergent mixture (*middle*) can be measured directly. The scattering profile of the PDC (*right*) has to be inferred using one of the approaches described in the text.

employed to deconvolve the PDC and micelle contributions.

Density Matching

One approach to separating the PDC and micelle scattering signals is to match the scattering density of the solvent to that of the detergent, such that the detergent micelles become invisible to the scattering experiments. These density-matching approaches were pioneered by Stuhrmann and coworkers in the 1960s and 1970s in SANS studies of globular proteins (90), lipids (45), and ribosomes (69). Due to the large difference of the neutron scattering cross-section between hydrogen and deuterium, the SANS scattering density can be adjusted over a wide range by changing the D_2O/H_2O ratio of the solution. Kendall and coworkers (15) employed density matching in SANS studies of nucleotide-binding-induced conformational changes of SecA in small unilamellar vesicles.

Bu & Engelman (14) have used sucrose solutions of different concentrations for density matching in SAXS experiments. They determined the R_g and the molecular weight of a model membrane protein system comprising human erythrocyte glycophorin A fused to the carboxyl terminus of monomeric staphylococcal nuclease in DDMAB micelles (14). However, density matching is far more difficult to achieve for SAXS than for SANS (90), as the relevant quantity in X-ray scattering is the electron density contrast, which is difficult to adjust without severely perturbing the biological system under study. Therefore, density matching in SAXS studies is limited to detergents that have a scattering contrast close to that of water.

Subtracting Micellar Scattering

A different approach to separating the contributions from PDC and micelle scattering is to record a scattering profile of the same detergent concentration in the absence of protein, which can be used to subtract out the contribution of the detergent micelle scattering. However, as an a priori unknown fraction of the detergent molecules becomes part of the PDC in the presence of protein, the concentration of empty detergent micelles will be different in the presence and absence of protein. This mismatch complicates the subtraction of the micelle contribution.

Scattering contrast: the scattering density (the electron density in the case of SAXS) of the macromolecule relative to that of the solvent

One strategy to achieve correct subtraction of the micelle signal is to extensively dialyze the sample against a buffer of known detergent concentration to ensure a fixed concentration of detergent micelles. Loll and coworkers (62) used this approach in light scattering studies. Extensive dialysis can be problematic, however, as for each PDC dialysis conditions need to be optimized and several days of dialysis are required.

Our lab has (19, 59) recently developed an approach that relies on considering two different limits for the background subtraction that provide an upper and lower bound for the forward scattering intensity $I(0)$ and R_g. This approximate treatment allows us to bracket the $I(0)$ and R_g of the PDC. In a recent study of eight integral membrane proteins from *Thermotoga maritima* in 11 different detergents, we found that the upper and lower bounds are close for 70–80% of protein-detergent combinations. In these cases reliable estimates could be obtained (70) for R_g and the protein oligomerization state. The advantage of this approximate treatment is that the R_g and the protein oligomerization state can be obtained from a single measurement of the protein sample without the need for dialysis. This approach is, therefore, well suited for high-throughput screening. However, it suffers from several shortcomings: (*a*) It works poorly for strongly scattering detergents; (*b*) it does not take into account particle interference effects; and (*c*) it only yields an approximation to the PDC scattering in the low-angle Guinier region, but fails at intermediate scattering angles, as most micelles have a characteristic scattering peak in this region (cf. red micelle scattering profile in **Figure 4**).

Singular value decomposition (SVD): factorization of a rectangular matrix that generalizes matrix diagonalization

Riboswitch: an RNA molecule that regulates gene expression through conformational changes induced by small-molecule ligand binding

Analysis of the PDC Scattering by Singular Value Decomposition

To address these shortcomings, we have developed a different approach that employs singular value decomposition (SVD) of scattering data collected at different (about 6 to 10) protein-detergent stoichiometries and a global fitting procedure (59). This approach is applicable even to strongly scattering detergents and determines the PDC scattering profile over the entire recorded momentum transfer range. Interparticle interference effects due to finite concentration are currently treated to second order in the PDC and micelle concentrations.

The determination of the full PDC scattering profile through SVD analysis of measurements at different protein-detergent stoichiometries provides information about the global shape and interactions of the PDC that is complementary to data obtained from NMR measurements (35). We anticipate that molecular modeling using input from both NMR and SAXS measurements will allow for more accurate membrane protein structure determination as well as a better understanding of protein-detergent interactions. Finally, knowledge about the interactions of PDCs in solution could help researchers to design better crystallization conditions (27, 65).

NUCLEIC ACIDS

The discovery of catalytic activity in RNA molecules by Cech, Altman, and coworkers in 1982 (32, 55) has led to considerable interest in the structure-function relationships of RNA molecules in biology. Furthermore, it is becoming clear that previously unknown RNA machinery, specified in the noncoding regions of the genome, is essential for controlling expression of genes. An example of such newly discovered RNA machines are riboswitches (64, 87). As in the case of protein science, X-ray crystallography is a powerful tool for RNA science. However, crystallography cannot be applied to fluctuating ensembles of unfolded or partially folded conformations. SAXS is one of the principal tools for obtaining low-resolution structural information on the conformations of folding intermediates of RNA molecules. At present the literature on these intermediates is confined mainly to the measurement of the R_g and the pair distribution function $p(r)$.

We have recently shown that 3-D reconstruction algorithms developed for protein systems can be applied successfully to RNA (58). **Figure 5** shows an example of an

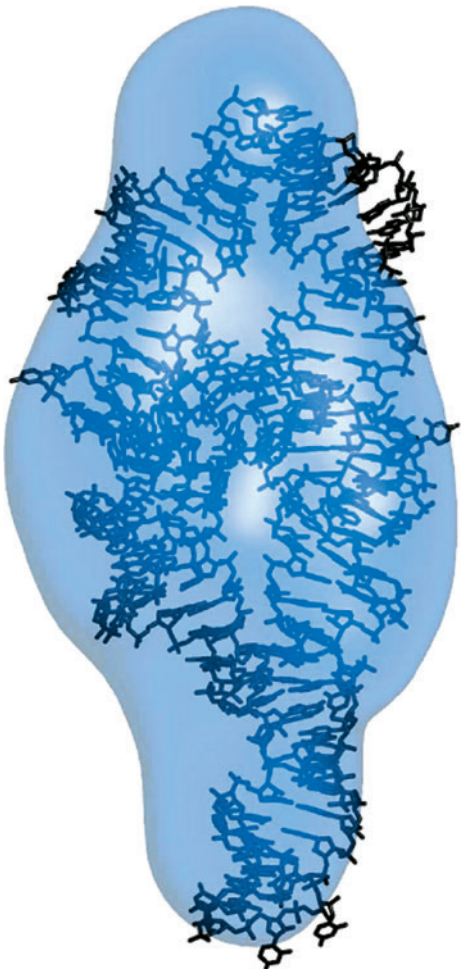

Figure 5

3-D reconstruction of the P4P6 domain of the *Tetrahymena* ribozyme (*blue*) superposed on the crystal structure (*black*) (58).

application of DAMMIN to RNA of a known crystal structure. The P4P6 domain of the *Tetrahymena* group I intron ribozyme has been reconstructed from scattering data. As may be seen from the figure, the shape determined from the 1-D SAXS measurements coincides well with that determined from the crystal structure (17). The availability of algorithms for 3-D reconstructions of RNA molecules from SAXS data enables researchers to obtain 3-D structural information on folding intermediates (60).

A complementary tool for structural studies of RNA folding intermediates has been hydroxyl radical footprinting (12, 56), in which the degree of solvent exposure can be assessed with single-residue resolution. Fenton chemistry or synchrotron radiation is used to generate hydroxyl radicals that cleave the RNA backbone. The amount of cleavage at each position in the RNA molecule is read out by gel electrophoresis and storage phosphor imaging of the radiolabeled RNA. Taken together, SAXS and hydroxyl radical footprinting are opening the way for detailed modeling of the RNA folding process and of its functional conformational changes.

The Forces that Drive RNA Folding

As RNA and DNA are highly negatively charged as a result of the phosphate-sugar backbone, the stabilization of compact RNA requires the presence of counterions that screen and neutralize the Coulomb repulsion due to the backbone. It has long been recognized that RNA folding proceeds differently from protein folding in that the secondary structure of RNA is already formed when the RNA chain is annealed at relatively low salt concentration (on the scale of 50 mM NaCl) at 50 to 90°C. In this initial stage the RNA has an extended conformation as a result of the poorly shielded strong electrostatic repulsion between the phosphates. Upon addition of millimolar concentrations of divalent counterions such as Mg^{2+} (106), (or molar concentrations of monovalent counterions in some cases) the RNA adopts a more compact conformation and, in the case of ribozymes, eventually folds to a functional catalytic state.

A model system approach to studying the effects of counterions was carried out by Bai et al. (4), who used SAXS to measure the salt dependence of the ensemble of conformations of a pair of 24-mer DNA duplexes tethered together by a short polyethylene glycol chain. While the strong shielding power of divalent counterions relative to that of the monovalents was seen in these measurements, the possible counterion-induced attraction, well known for higher valence polyamines inducing DNA condensation, was not induced by the addition of Mg^{2+} within the accuracy of the measurements.

Use of SAXS to Characterize RNA Folding Intermediates

Russell et al. (76–78) used time-resolved SAXS to study the time course of compaction of the group I intron ribozyme from *Tetrahymena*. It was found that several stages could be identified along the folding pathway and could be correlated with structural intermediates that had been studied using hydroxyl radical footprinting by Brenowitz and coworkers (80). The initial collapse was measured to take place on a timescale of a few milliseconds and led to a compact intermediate state. This initial collapsed state lasted for times on the order of 100 ms before further folding took place, leading eventually to a functional state on a timescale of about 100 s. The initial collapse can be triggered by high concentrations of monovalent ions (roughly 1M KCl); however, the fully functional state could only be attained by adding millimolar magnesium concentrations.

A subsequent SAXS measurement of a quintuple mutant designed to destabilize the tertiary contacts present in the folded state of the ribozyme (23) showed that collapse to the initial compact intermediate upon addition of salt occurs even in the absence of these specific tertiary interactions. The experiments led to

Anomalous small-angle X-ray scattering: a variation of the SAXS technique that exploits the change in scattering properties with photon energy around atomic resonances

the conclusion that the initial compaction is a result of nonspecific shielding of the Coulomb forces by the added counterions. The subsequent compaction on the timescale of 100 ms, however, is suggested to be stabilized partly by tertiary hydrogen bond contacts that are not present in the mutant case. From a SAXS measurement point of view, the fully compact folded state could be achieved by a high concentration of monovalent salt. However, crystallographic studies have shown that the occupation of six specific magnesium binding sites is necessary for the catalytic functionality of the ribozyme. Thus, in addition to the shielding of the Coulomb forces by the counterion atmosphere, specific magnesium binding is needed to stabilize the fully functional conformation of the ribozyme.

In a recent study by Sosnick and collaborators (5) the use of SAXS, partial nucleolysis, and circular dichroism led to the structural characterization of a folding intermediate for the specificity (S-)domain of the *Bacillus subtilis* RNase P ribozyme. The crystal structure of the fully folded state of this domain of the ribozyme contained four tertiary structural modules: a rigid core, a four-way junction, a tetra-loop receptor, and an unusual motif involving two tertiary interacting loops (52). In the thermodynamic folding pathway, which was studied by titration against Mg^{2+}, a structural intermediate I_{eq} was populated. The size and shape of the native and I_{eq} intermediate structures are characterized by SAXS measurements. The R_g and $p(r)$ for the native structure obtained from SAXS are in good agreement with those calculated from the crystal structure. The R_g for the intermediate is 8.8 Å bigger than that for the native (32.2 Å), and $p(r)$ analysis indicates that I_{eq} has a more extended shape (a maximum dimension of 135 Å) compared with the native structure (110 Å). Starting with the atomic model of the native state obtained from crystallography, Sosnick et al. have generated a candidate structural model for I_{eq} by a series of molecular mechanics transformations. In order to achieve a ΔR_g value that approaches that measured by SAXS, modular rearrangements require that both the P 10.1 and the P 12 duplexes are extended in opposite directions. The possible alternative structures within this value of ΔR_g are limited so that the authors are able to conclude that the global arrangement with P 10.1 and P 12 splayed out in opposite directions is the major structural feature consistent with the SAXS and hydroxy radical data for $I_{eq.}$

Exploring the Thermodynamic Landscape of a Riboswitch

In a SAXS study of the structural intermediate for a glycine riboswitch, Lipfert et al. (60) mapped out the conformational landscape of the molecule as a function of both Mg^{2+} and glycine concentrations. Going from low salt conditions to high Mg^{2+} (10 mM) conditions, the molecule underwent a partial folding transition associated with significant conformational changes and compaction. The addition of glycine in the presence of millimolar Mg^{2+} led to further conformational changes and compaction upon glycine binding. Thermodynamic modeling indicated that the second transition from the conformation in high Mg^{2+} alone to the glycine-bound state required the association of additional Mg^{2+} ions. Using 3-D reconstruction algorithms, low-resolution models of all three thermodynamic states (the low salt or unfolded state, the compact intermediate, and the fully folded and glycine-bound state) could be obtained.

Use of Anomalous SAXS to Study the Distribution of the Ion Atmosphere

In the dilute limit, where SAXS is not complicated by interparticle interference, Das et al. (24) used anomalous SAXS to study the radial distribution function of counterions around a small DNA duplex. By using the anomalous absorption edges at 15.1 keV for monovalent rubidium, and 16.1 keV for divalent strontium, Das et al. saw the change in radial distribution functions between the

monovalent and divalent ion atmospheres around a DNA duplex. As expected from Poisson-Boltzmann (PB) theory, the radial distribution function is much more compact for the divalents (typically falls off on the scale of the Bjerrum length of around 7 Å) than for the monovalents, which is determined by the Debye screening length, inversely proportional to the square root of the ion concentration. In a follow-up study, however, systematic deviations from simple PB theory were observed (1). These deviations likely stem from ion size and correlation effects, which are neglected in the mean-field PB treatment.

UNFOLDED PROTEINS AND PEPTIDES

The study of unfolded ensembles of proteins is of interest for several reasons. Fundamentally, the unfolded ensemble constitutes one half of the protein folding paradigm; any description of protein folding therefore must include the unfolded state. Furthermore, an increasing number of proteins are natively unfolded (29). These natively unfolded proteins are involved in a range of cellular functions and often become folded when in contact with a substrate that may be a another protein, peptide, nucleic acid, or lipid vesicle. Finally, unfolded or misfolded proteins are involved in a range of pathologies, such as amyloid formation in neuropathologies (40).

Evidence for Random Coil Behavior

The majority of expressed proteins are naturally folded in solution and can be unfolded by the addition of denaturants, generally urea or guanidine hydrochloride (GuHCl), raising the temperature (or lowering it in the case of cold denaturation), or various other means. Early measurements of intrinsic viscosity and optical dispersion of proteins in 6 M GuHCl by Tanford et al. (98, 99) suggested that unfolded proteins behave as random coils and retain no elements of their native conformation. In agreement with these early results, recent systematic SAXS studies of denatured proteins (16, 47, 67, 73) found that the R_g depends on chain length (number of residues N), as expected for a self-avoiding random walk:

$$R_g = AN^{\nu}. \qquad 3.$$

Here the exponent ν is close to $\nu = 3/5$, consistent with Flory's theory. However, the prefactor A, which is empirically of the order 1.9 Å, seems anomalously small since it is expected to measure the persistence length of the polypeptide chain, which by Flory's estimate should be on the scale of 6 to 8 Å.

PB: Poisson-Boltzmann

GuHCl: guanidine hydrochloride

Residual Structure and the Reconciliation Problem

In contrast, recent NMR studies suggest that even highly denatured proteins have considerable residual structure, possibly even encoding native-like topology (86). Kristjansdottir et al. (54) observed long-range interactions in denatured acyl coenzyme A binding protein at a variety of denaturant concentrations using paramagnetic relaxation enhancement studies, which are similar to interactions present under native conditions, though they become weaker as the GuHCl concentrations are increased. The apparent contradiction between significant amounts of local structure and global random coil behavior is the so-called reconciliation problem (66, 74).

A similar apparent contradiction was observed in studies of the 11-residue, poly-alanine model peptide XAO. XAO is essentially too short to fold even under non-denaturing conditions. Using spectroscopic studies, Shi et al (85) suggested XAO has significant polyproline II (PPII) structural content. In contrast, molecular dynamics simulations predict significant α-helical content for most standard force fields (111). However, both PPII and α-helical conformations are irreconcilable with the R_g of 7.4 ± 0.5 Å determined by SAXS (111). In a combined NMR and simulation study Scheraga and coworkers (63) found XAO to populate a conformational ensemble consistent with the R_g value

Kratky plot: representation of scattering intensity weighted by the momentum transfer squared

from SAXS, for which the PPII conformation is only one of many conformational states.

Two recent studies proposed methods to generate unfolded protein ensembles in Monte Carlo procedures by sampling backbone dihedral angles from loop regions of proteins in the Protein Data Bank (8) and by imposing additional excluded volume constraints (9, 44). Bernadó et al. (9) proposed a model for the partially folded nucleocapsid binding domain of Sendai virus phosphoprotein in agreement with residual dipolar coupling and SAXS data. Jha et al. (44) generated models for a range of proteins. Their models contain significant amounts of local backbone structure, in agreement with residual dipolar coupling data, but remarkably also fit the global scaling law for the R_g versus number of residues given by Equation 3, with values for the constant A of the order 1.9–2.4 Å. Interestingly, their models do not display evidence of native-like topology.

SAXS as a Tool to Test Models of Unfolded Protein Ensembles

It seems likely that further work using the entire recorded q-range of SAXS profiles of highly denatured proteins (going beyond R_g measurements) to test different models of unfolded proteins would help to resolve some of these differences and to provide a more stringent test of models than simple scaling laws alone. Early SAXS studies of the refolding of cytochrome c by Segel et al. (81, 82) indicated that at high GuHCl concentration the SAXS data shows a typical rising tail in the Kratky plot (a plot of $q^2 I$ as a function of q), characteristic of a random coil (26). However, on lowering the GuHCl concentration, the Kratky plot started to show evidence of a more compact state, even though the R_g had not changed appreciably. Preliminary results for the XAO peptide indicate deviations of the SAXS profiles computed from the ensemble generated by Scheraga and coworkers and of the measured SAXS profiles at high q. There is a general tendency for models of unfolded protein ensembles to systematically underestimate the scattering intensity in the high q region of SAXS measurements (110; J. Lipfert & S. Doniach, unpublished results). It will be important to determine whether these deviations are due to shortcomings of the model ensembles or to an inaccurate treatment of solvent scattering for the unfolded protein structures.

OUTLOOK

The availability of high-brilliance X-ray sources is going to substantially increase in the near future, with the ongoing construction of the new synchrotron facilities Diamond in the United Kingdom. (**http://www.diamond.ac.uk/default.htm**) and Soleil in France (**http://www.synchrotron-soleil.fr/**) and upgrades to, among others, the DESY/HASYLAB facility in Germany and to the Advanced Photon Source, Stanford Synchrotron Radiation Laboratory, and Advanced Light Source SAXS beam lines in the United States. Since radiation damage is already a limiting factor for measurements at state-of-the-art third-generation synchrotron beam lines, higher X-ray flux is primarily beneficial for time-resolved measurements.

Many macromolecules of biological interest are difficult and costly to make in large quantities; therefore, reducing the sample volumes required for SAXS measurements is an important concern. Currently, measurements with ≈15 μl are possible (61) and further miniaturization seems feasible. Equally important are further automation of sample loading and data analysis procedures, as at high-flux synchrotrons these steps already take significantly longer than the actual scattering measurement.

New algorithms, such as the 3-D modeling programs described in this review, are helping to automate the interpretation of the data and to maximize the information that can be extracted from a SAXS profile. The integration of data from different techniques [such as NMR (35), footprinting and mass spectrometry (97), and fluorescence techniques]

in molecular modeling approaches will be an important challenge.

An exciting new approach is the use of site-specific-attached gold nanocrystals as markers in biological SAXS experiments. The interference between the gold nanocrystals can be used to obtain molecular distance distributions, thus providing an absolute molecular ruler (R.S. Mathew-Fenn, R. Das & P.B. Harbury, manuscript submitted).

SUMMARY POINTS

1. SAXS is a solution scattering technique that enables studies of biological macromolecules under a wide variety of solution conditions, from near physiological to highly denaturing.
2. Ab initio reconstruction algorithms allow one to obtain low-resolution 3-D density maps from 1-D scattering data.
3. An important application of SAXS is the modeling of macromolecular complexes. Model building is greatly facilitated if prior information (e.g., high-resolution structures of individual components) is available.
4. Membrane protein-detergent complexes are an emerging target for SAXS studies.
5. SAXS is an important technique to study protein and RNA folding, as the overall conformation of a macromolecule can be followed as a function of time, salt, or denaturant concentration.
6. Ensembles of partially or fully unfolded proteins or nucleic acids can be characterized structurally at a global level using SAXS.

ACKNOWLEDGMENTS

The authors thank Marc Delarue, Linda Columbus, Sönke Seifert, Marc Niebuhr, and Rebecca S. Mathew-Fenn for useful discussions, and Joanna Makowska and Harold A. Scheraga for providing the Protein Data Bank files of their ensemble of XAO structures. This research was supported by the National Science Foundation grant PHY-0140140 and the National Institutes of Health grant PO1 GM0066275.

LITERATURE CITED

1. Andresen K, Das R, Park HY, Smith H, Kwok LW, et al. 2004. Spatial distribution of competing ions around DNA in solution. *Phys. Rev. Lett.* 93(24):248103
2. Aparicio R, Fischer H, Scott DJ, Verschueren KHG, Kulminskaya AA, et al. 2002. Structural insights into the beta-mannosidase from *T. reesei* obtained by synchrotron small-angle X-ray solution scattering enhanced by X-ray crystallography. *Biochemistry* 41(30):9370–75
3. Bada M, Walther D, Arcangioli B, Doniach S, Delarue M. 2000. Solution structural studies and low-resolution model of the *Schizosaccharomyces pombe* SAP-1 protein. *J. Mol. Biol.* 300(3):563–74
4. Bai Y, Das R, Millett IS, Herschlag D, Doniach S. 2005. Probing counterion modulated repulsion and attraction between nucleic acid duplexes in solution. *Proc. Natl. Acad. Sci. USA* 102(4):1035–40

5. Baird NJ, Westhof E, Qin H, Pan T, Sosnick TR. 2005. Structure of a folding intermediate reveals the interplay between core and peripheral elements in RNA folding. *J. Mol. Biol.* 352(3):712–22
6. Bendedouch D, Chen S-H, Koehler WC. 1983. Determination of interparticle structure factors in ionic micellar solutions by small angle neutron scattering. *J. Phys. Chem.* 87:2621–28
7. Beno MA, Jennings G, Engbretson M, Knapp GS, Kurtz C, et al. 2001. Basic Energy Sciences Synchrotron Radiation Center undulator sector at the advanced photon source. *Nucl. Instrum. Methods Phys. Res. A* 467–468:690–93
8. Berman HM, Westbrook J, Feng Z, Gilliland G, Bhat TN, et al. 2000. The Protein Data Bank. *Nucleic Acids Res.* 28(1):235–42
9. Bernadó P, Blanchard L, Timmins P, Marion D, Ruigrok RWH, Blackledge M. 2005. A structural model for unfolded proteins from residual dipolar couplings and small-angle X-ray scattering. *Proc. Natl. Acad. Sci. USA* 102(47):17002–7
10. Bezzobotnov VY, Borbély S, Cser L, Faragó B, Gladkih IA, et al. 1988. Temperature and concentration dependence of properties of sodium dodecyl sulfate micelles determined from small-angle neutron scattering experiments. *J. Phys. Chem.* 92:5738–43
11. Bouwstra JA, Gooris GS, Bras W, Talsma H. 1993. Small angle X-ray scattering: possibilities and limitations in characterization of vesicles. *Chem. Phys. Lipids* 64(1–3):83–98
12. Brenowitz M, Chance MR, Dhavan G, Takamoto K. 2002. Probing the structural dynamics of nucleic acids by quantitative time-resolved and equilibrium hydroxyl radical "footprinting." *Curr. Opin. Struct. Biol.* 12:648–53
13. Brzustowicz MR, Brunger AT. 2005. X-ray scattering from unilamellar lipid vesicles. *J. Appl. Crystallogr.* 38:126–31

14. First study of a membrane protein system with SAXS using density matching.

14. Bu Z, Engelman DM. 1999. A method for determining transmembrane helix association and orientation in detergent micelles using small angle X-ray scattering. *Biophys. J.* 77:1064–73

15. Bu Z, Wang L, Kendall DA. 2003. Nucleotide binding induces changes in the oligomeric state and conformations of SecA in a lipid environment: a small-angle neutron-scattering study. *J. Mol. Biol.* 332:23–30
16. Calmettes P, Roux B, Durand D, Desmadril M, Smith JC. 1993. Configurational distribution of denatured phosphoglycerate kinase. *J. Mol. Biol.* 231(3):840–48
17. Cate JH, Gooding AR, Podell E, Zhou K, Golden B, et al. 1996. Crystal structure of a group I ribozyme domain: principles of RNA packing. *Science* 273:1678–85

18. First description of a bead reconstruction algorithm for SAXS data.

18. Chacon P, Moran F, Diaz JF, Pantos E, Andreu JM. 1998. Low-resolution structures of proteins in solution retrieved from X-ray scattering with a genetic algorithm. *Biophys. J.* 74:2760–75

19. Columbus L, Lipfert J, Klock H, Millett IS, Doniach S, Lesley S. 2006. Expression, purification and characterization of *Thermotoga maritima* α-helical membrane proteins for structure determination. *Protein Sci.* 15:961–75
20. Corbett KD, Shultzaberger RK, Berger JM. 2004. The C-terminal domain of DNA gyrase A adopts a DNA-bending beta-pinwheel fold. *Proc. Natl. Acad. Sci. USA* 101(19):7293–98
21. Costenaro L, Grossmann JG, Ebel C, Maxwell A. 2005. Small-angle X-ray scattering reveals the solution structure of the full-length DNA gyrase A subunit. *Structure* 13(2):287–96
22. Dainese E, Sabatucci A, van Zadelhoff G, Angelucci CB, Vachette P, et al. 2005. Structural stability of soybean lipoxygenase-1 in solution as probed by small angle X-ray scattering. *J. Mol. Biol.* 349(1):143–52

23. Das R, Kwok LW, Millet IS, Bai Y, Mills T, et al. 2003. The fastest global events in RNA folding: electrostatic relaxation and tertiary collapse of the *Tetrahymena* ribozyme. *J. Mol. Biol.* 332:311–19
24. Das R, Mills TT, Kwok LW, Maskel GS, Millett IS, et al. 2003. Counterion distribution around DNA probed by solution X-ray scattering. *Phys. Rev. Lett.* 90:1881031–34
25. Denisov IG, Grinkova YV, Lazarides AA, Sligar SG. 2004. Directed self-assembly of monodisperse phospholipid bilayer nanodiscs with controlled size. *J. Am. Chem. Soc.* 126(11):3477–87
26. Doniach S. 2001. Changes in biomolecular conformations seen by small angle X-ray scattering. *Chem. Rev.* 101:1763–78
27. Ducruix A, Guilloteau JP, Riès-Kautt M, Tardieu A. 1996. Protein interactions as seen by solution X-ray scattering prior to crystallogenesis. *J. Crystallogr. Growth* 168:28–39
28. Dupuy C, Auvray X, Petipas C, Rico-Lattes I, Lattes A. 1997. Anomeric effects on the structure of micelles of alkyl maltosides in water. *Langmuir* 13:3965–67
29. Dyson HJ, Wright PE. 2005. Intrinsically unstructured proteins and their functions. *Nat. Rev. Mol. Cell. Biol.* 6(3):197–208
30. Egea PF, Rochel N, Birck C, Vachette P, Timmins PA, Moras D. 2001. Effects of ligand binding on the association properties and conformation in solution of retinoic acid receptors RXR and RAR. *J. Mol. Biol.* 307(2):557–76
31. Fujisawa T, Kostyukova A, Maeda Y. 2001. The shapes and sizes of two domains of tropomodulin, the P-end-capping protein of actin-tropomyosin. *FEBS Lett.* 498(1):67–71
32. Gesteland RF, Cech T, Atkins JF. 2006. *The RNA World*. Cold Spring Harbor, NY: Cold Spring Harbor Lab. Press
33. Gherardi E, Sandin S, Petoukhov MV, Finch J, Youles ME, et al. 2006. Structural basis of hepatocyte growth factor/scatter factor and MET signaling. *Proc. Natl. Acad. Sci. USA* 103(11):4046–51
34. Glatter O, Kratky O. 1982. Small angle X-ray scattering. London: Academic
35. Grishaev A, Wu J, Trewhella J, Bax A. 2005. Refinement of multidomain protein structures by combination of solution small-angle X-ray scattering and NMR data. *J. Am. Chem. Soc.* 127(47):16621–28
36. Grossmann JG. 2007. Biological solution scattering: recent achievements and future directions. *J. Appl. Crystallogr.* In press
37. Guinier A. 1939. La diffraction des rayons X aux très petits angles: application à l'étude de phénomènes ultramicroscopiques. *Ann. Phys.* 12:161–237
38. Hammel M, Walther M, Prassl R, Kuhn H. 2004. Structural flexibility of the N-terminal beta-barrel domain of 15-lipoxygenase-1 probed by small angle X-ray scattering. Functional consequences for activity regulation and membrane binding. *J. Mol. Biol.* 343(4):917–29
39. Hansen JP, Hayter JB. 1981. A rescaled MSA structure factor for dilute charged colloidal dispersions. *Mol. Phys.* 46:651–56
40. Harper JD, Lansbury PT. 1997. Models of amyloid seeding in Alzheimer's disease and scrapie: mechanistic truths and physiological consequences of time-dependent solubility of amyloid proteins. *Annu. Rev. Biochem.* 66:385–407
41. Hayter JB, Penfold J. 1981. An analytic structure factor for macroion solutions. *Mol. Phys.* 42(1):109–18
42. Hayter JB, Zemb T. 1982. Concentration-dependent structures of sodium octanoate micelles. *Chem. Phys. Lett.* 93(1):91–94

24. First use of anomalous SAXS to study the ion atmosphere around a DNA molecule.

43. He Z, Garamus VM, Funari SS, Malfois M, Willumeit R, Niemeyer B. 2002. Comparison of small-angle scattering methods for the structural analysis of octyl-β-maltopyranoside micelles. *J. Phys. Chem. B* 106:7596–604
44. Jha AK, Colubri A, Freed KF, Sosnick TR. 2005. Statistical coil model of the unfolded state: resolving the reconciliation problem. *Proc. Natl. Acad. Sci. USA* 102(37):13099–104
45. Knoll W, Haas J, Stuhrmann HB, Fuldner HH, Vogel H, Sackmann E. 1981. Small-angle neutron scattering of aqueous dispersions of lipids and lipid mixtures. A contrast variation study. *J. Appl. Crystallogr*. 14(3):191–202

46. Comprehensive review of SAXS theory and applications.

46. Koch MHJ, Vachette P, Svergun DI. 2003. Small-angle scattering: a view on the properties, structures and structural changes of biological macromolecules in solution. *Q. Rev. Biophys*. 36(2):147–27

47. This study of denatured proteins shows that the R_gs follow a scaling law with an exponent characteristic of a self-avoiding random walk.

47. Kohn JE, Millett IS, Jacob J, Zagrovic B, Dillon TM, et al. 2004. Random-coil behavior and the dimensions of chemically unfolded proteins. *Proc. Natl. Acad. Sci. USA* 101(34):12491–96

48. Korepanova A, Gao FP, Hua Y, Qin H, Nakamoto RK, Cross TA. 2005. Cloning and expression of multiple integral membrane proteins from *Mycobacterium tuberculosis* in *Escherichia coli*. *Protein Sci*. 14:148–58
49. Kozin MB, Svergun DI. 1997. ASSA, a program for the three-dimensional rendering in solution scattering from biopolymers. *J. Appl. Crystallogr*. 30:811–15
50. Kozin MB, Svergun DI. 2000. A software system for rigid-body modelling of solution scattering data. *J. Appl. Crystallogr*. 33:775–77
51. Kozin MB, Svergun DI. 2001. Automated matching of high- and low-resolution structural models. *J. Appl. Crystallogr*. 34:33–41
52. Krasilnikov AS, Yang X, Pan T, Mondragon A. 2003. Crystal structure of the specificity domain of ribonuclease P. *Nature* 421(6924):760–64
53. Kretchetov A. 2005. *Reconstruction of three-dimensional electron density models from small angle X-ray scattering data for macromolecules. A space averaging approach*. PhD thesis. Stanford Univ.
54. Kristjansdottir S, Lindorff-Larsen K, Fieber W, Dobson CM, Vendruscolo M, Poulsen FM. 2005. Formation of native and non-native interactions in ensembles of denatured ACBP molecules from paramagnetic relaxation enhancement studies. *J. Mol. Biol*. 347(5):1053–62
55. Kruger K, Grabowski PJ, Zaug AJ, Sands J, Gottschling DE, Cech TR. 1982. Self-splicing RNA: autoexcision and autocyclization of the ribosomal RNA intervening sequence of *Tetrahymena*. *Cell* 31(1):147–57
56. Latham JA, Cech TR. 1989. Defining the inside and outside of a catalytic RNA molecule. *Science* 245:276–82
57. Lin TL, Chen S-H, Gabriel NE, Roberts MF. 1986. Use of small-angle neutron scattering to determine the structure and interaction of dihexanoylphosphatidylcholine micelles. *J. Am. Chem. Soc*. 108:3499–507
58. Lipfert J, Chu VB, Bai Y, Herschlag D, Doniach S. 2007. Low resolution models for nucleic acids from small-angle X-ray scattering with applications to electrostatic modeling. *J. Appl. Crystallogr*. In press
59. Lipfert J, Columbus L, Chu VB, Doniach S. 2007. Analysis of small-angle X-ray scattering data of protein-detergent complexes by singular value decomposition. *J. Appl. Crystallogr*. In press

60. First use of SAXS to study Mg^{2+}-dependent folding and ligand binding for a riboswitch.

60. Lipfert J, Das R, Chu VB, Kudaravalli M, Boyd N, et al. 2006. Structural transitions and thermodynamics of a glycine-dependent riboswitch from *Vibrio cholerae*. *J. Mol. Biol*. 365:1393–406

61. Lipfert J, Millett IS, Seifert S, Doniach S. 2006. A sample holder for small-angle X-ray scattering static and flow cell measurements. *Rev. Sci. Instrum*. 77:461081–84
62. Loll PJ, Allaman M, Wiencek J. 2001. Assessing the role of detergent-detergent interactions in membrane protein crystallization. *J. Crystallogr. Growth* 232:432–38
63. Makowska J, Rodziewicz-Motowidlo S, Baginska K, Vila JA, Liwo A, et al. 2006. Polyproline II conformation is one of many local conformational states and is not an overall conformation of unfolded peptides and proteins. *Proc. Natl. Acad. Sci. USA* 103:1744–49
64. Mandal M, Breaker RR. 2004. Gene regulation by riboswitches. *Nat. Rev. Mol. Cell. Biol.* 5:451–63
65. Marone PA, Thiyagarajan P, Wagner AM, Tiede DM. 1999. Effect of the alkyl chain length on crystallization of a detergent-solubilized membrane protein: correlation of protein-detergent particle size and particle-particle interaction with crystallization of the photosynthetic reaction center from *Rhodobacter sphaeroides*. *J. Crystallogr. Growth* 207:214–25
66. McCarney ER, Kohn JE, Plaxco KW. 2005. Is there or isn't there? The case for (and against) residual structure in chemically denatured proteins. *Crit. Rev. Biochem. Mol. Biol.* 40(4):181–89 [CLEO: Reference 20 and 102]
67. Millett IS, Doniach S, Plaxco KW. 2002. Toward a taxonomy of the unfolded state: small angle scattering studies of unfolded proteins. *Adv. Protein Chem*. 62:241–62
68. Morais Cabral JH, Jackson AP, Smith CV, Shikotra N, Maxwell A, Liddington RC. 1997. Crystal structure of the breakage-reunion domain of DNA gyrase. *Nature* 388(6645):903–1006
69. Parfait R, Koch MHJ, Haas J, Stuhrmann HB, Crichton RR. 1978. Neutron small-angle scattering of *E. coli* ribosomes. A contrast variation study. *J. Appl. Crystallogr*. 11(5):487–88
70. Petoukhov MV, Eady NAJ, Brown KA, Svergun DI. 2002. Addition of missing loops and domains to protein models by X-ray solution scattering. *Biophys. J*. 83(6):3113–25
71. Petoukhov MV, Svergun DI. 2003. New methods for domain structure determination of proteins from solution scattering data. *J. Appl. Crystallogr*. 36:540–44
72. Petoukhov MV, Svergun DI. 2005. Global rigid body modeling of macromolecular complexes against small-angle scattering data. *Biophys. J*. 89(2):1237–50
73. Petrescu AJ, Receveur V, Calmettes P, Durand D, Desmadril M, et al. 1997. Small-angle neutron scattering by a strongly denatured protein: analysis using random polymer theory. *Biophys. J*. 72(1):335–42
74. Plaxco KW, Gross M. 2001. Unfolded, yes, but random? Never! *Nat. Struct. Biol.* 8(8):659–60
75. Rosenberg OS, Deindl S, Sung RJ, Nairn AC, Kuriyan J. 2005. Structure of the autoinhibited kinase domain of CaMKII and SAXS analysis of the holoenzyme. *Cell* 123(5):849–60
76. Russell R, Millett IS, Doniach S, Herschlag D. 2000. Small angle X-ray scattering reveals a compact intermediate in RNA folding. *Nat. Struct. Biol*. 7(5):367–70
77. Russell R, Millett IS, Tate MW, Kwok LW, Nakatani B, et al. 2002. Rapid compaction during RNA folding. *Proc. Natl. Acad. Sci. USA* 99(7):4266–71
78. Russell R, Zhuang X, Babcock HP, Millett IS, Doniach S, et al. 2002. Exploring the folding landscape of a structured RNA. *Proc. Natl. Acad. Sci. USA* 99(1):155–60
79. Sanders CR, Sonnichsen F. 2006. Solution NMR of membrane proteins: practice and challenges. *Magn. Reson. Chem*. 44:24–40
80. Sclavi B, Sullivan M, Chance MR, Brenowitz M, Woodson SA. 1998. RNA folding at millisecond intervals by synchrotron hydroxyl radical footprinting. *Science* 279(5358):1940–43

81. Segel DJ, Eliezer D, Uversky V, Fink AL, Hodgson K, Doniach S. 1999. Transient dimer in the refolding kinetics of cytochrome *c* characterized by small-angle X-ray scattering. *Biochemistry* 38:15352–59

82. Nice treatment of how SVD can be used to study folding intermediates.

82. Segel DJ, Fink AL, Hodgson KO, Doniach S. 1998. Protein denaturation: a small-angle X-ray scattering study of the ensemble of unfolded states of cytochrome *c*. *Biochemistry* 37:12443–51

83. Seifert S, Winans RE, Tiede DM, Thiyagarajan P. 2000. Design and performance of a ASAXS instrument at the advanced photon source. *J. Appl. Crystallogr*. 33:782–84

84. Shi Z, Chen K, Liu Z, Kallenbach NR. 2006. Conformation of the backbone in unfolded proteins. *Chem. Rev*. 106(5):1877–97

85. Shi Z, Olson CA, Rose GD, Baldwin RL, Kallenbach NR. 2002. Polyproline II structure in a sequence of seven alanine residues. *Proc. Natl. Acad. Sci. USA* 99:9190–95

86. Shortle D, Ackerman MS. 2001. Persistence of native-like topology in a denatured protein in 8 M urea. *Science* 293(5529):487–89

87. Soukup JK, Soukup GA. 2004. Riboswitches exert genetic control through metabolite-induced conformational change. *Curr. Opin. Struct. Biol*. 14(3):344–49

88. Stuhrmann HB. 1970. Interpretation of small-angle scattering functions of dilute solutions and gases. A representation of the structures related to a one-particle-scattering function. *Acta Crystallogr. A* 26:297–306

89. Stuhrmann HB. 1970. New method for determination of surface form and internal structure of dissolved globular proteins from small-angle X-ray measurements. *Z. Phys. Chem*. 72:177

90. Stuhrmann HB, Miller A. 1978. Small-angle scattering of biological structures. *J. Appl. Crystallogr*. 11(5):325–45

91. Svergun DI. 1992. Determination of the regularization parameter in indirect-transform methods using perceptual criteria. *J. Appl. Crystallogr*. 25:495–503

92. Describes a method using simulated annealing for ab initio 3-D shape reconstruction, implemented in the program DAMMIN.

92. Svergun DI. 1999. Restoring low resolution structure of biological macromolecules from solution scattering using simulated annealing. *Biophys. J.* 76:2879–86

93. Comprehensive review of SAXS theory and applications.

93. Svergun DI, Koch MHJ. 2003. Small-angle scattering studies of biological macromolecules in solution. *Rep. Prog. Phys*. 66:1735–82

94. Describes a method for ab initio shape reconstruction for proteins implemented in the program GASBOR.

94. Svergun DI, Petoukhov MV, Koch MH. 2001. Determination of domain structure of proteins from X-ray solution scattering. *Biophys. J.* 80(6):2946–53

95. Svergun DI, Stuhrmann HB. 1991. New developments in direct shape determination from small-angle X-ray scattering. 1. Theory and model-calculations. *Acta Crystallogr. A* 47:736–44

96. Takahashi Y, Nishikawa Y, Fujisawa T. 2003. Evaluation of three algorithms for ab initio determination of three-dimensional shape from one-dimensional solution scattering profiles. *J. Appl. Crystallogr*. 36:549–52

97. Takamoto K, Chance MR. 2006. Radiolytic protein footprinting with mass spectrometry to probe the structure of macromolecular complexes. *Annu. Rev. Biophys. Biomol. Struct*. 35:251–76

98. Tanford C, Kawahara K, Lapanje S. 1966. Proteins in 6-M guanidine hydrochloride. Demonstration of random coil behavior. *J. Biol. Chem*. 241(8):1921–23

99. Tanford C, Kawahara K, Lapanje S. 1967. Proteins as random coils. I. intrinsic viscosities and sedimentation coefficients in concentrated guanidinium hydrochloride. *J. Am. Chem. Soc*. 89(4):729–36

100. Thiyagarajan P, Tiede DM. 1994. Detergent micelle structure and micelle-micelle interactions determined by small-angle neutron scattering under solution conditions used for membrane protein crystallization. *J. Phys. Chem*. 98:10343–51
101. Tikhonov A, Arsenin V. 1977. *Solution of Ill-Posed Problems*. New York: Wiley
102. Volkov VV, Svergun DI. 2003. Uniqueness of *ab initio* shape determination in small-angle scattering. *J. Appl. Crystallogr*. 36:860–64
103. Wallin E, von Heijne G. 1998. Genome-wide analysis of integral membrane proteins from eubacterial, archaean, and eukaryotic organisms. *Protein Sci*. 7:1029–38
104. Walther D, Cohen FE, Doniach S. 2000. Reconstruction of low resolution three-dimensional density maps from one-dimensional small angle X-ray scattering data for biomolecules in solution. *J. Appl. Crystallogr*. 33:350–63
105. White SH, Wimley WC. 1999. Membrane protein folding and stability: physical principles. *Annu. Rev. Biophys. Biomol. Struct*. 28:319–65
106. Woodson SA. 2005. Metal ions and RNA folding: a highly charged topic with a dynamic future. *Curr. Opin. Chem. Biol*. 9:104–9
107. Wriggers W, Chacón P. 2001. Using Situs for the registration of protein structures with low-resolution bead models from X-ray solution scattering. *J. Appl. Crystallogr*. 34:773–76
108. Wriggers W, Milligan RA, McCammon JA. 1999. Situs: a package for docking crystal structures into low-resolution maps from electron microscopy. *J. Struct. Biol*. 125:185–95
109. Wu Y, Tian X, Lu M, Chen M, Qinghua W, Ma J. 2005. Folding of small helical proteins assisted by small-angle X-ray scattering profiles. *Structure* 13:1587–97
110. Zagrovic B, Jayachandran G, Millett IS, Doniach S, Pande VS. 2005. How large is an α-helix? Studies of the radii of gyration of helical peptides by small-angle X-ray scattering and molecular dynamics. *J. Mol. Biol*. 353:232–41
111. Zagrovic B, Lipfert J, Sorin EJ, Millett IS, van Gunsteren WF, et al. 2005. Unusual compactness of a polyproline type II structure. *Proc. Natl. Acad. Sci. USA* 102(33):11698–703
112. Zhang R, Marone PA, Thiyagarajan P, Tiede DM. 1999. Structure and molecular fluctuations of N-alkyl-β-D-glucopyranoside micelles determined by X-ray and neutron scattering. *Langmuir* 15:7510–19
113. Zheng W, Doniach S. 2002. Protein structure prediction constrained by solution X-ray scattering data and structural homology identification. *J. Mol. Biol*. 316(1):173–87